JOURNAL OF GUIDANCE, CONTROL, AND DYNAMICS
Vol. 16, No. 1, January-February 1993

Precision Attitude Control for Tethered Satellites

Robert J. Kline-Schoder*
Lockheed Research Laboratory, Palo Alto, California 94304
and
J. David Powell†
Stanford University, Stanford, California 94305

Tethered spacecraft are particularly well suited to serve as isolation platforms for space-borne observatories. It has previously been shown that, due to the relatively large tether force, conventional means of performing attitude control for tethered satellites are inefficient for any mission with pointing requirements more stringent than about 1 deg. A particularly effective method of implementing attitude control for tethered satellites is to use the tether tension force to generate control moments by moving the tether attach point relative to the subsatellite center of mass. This paper presents the development of a precision pointing control algorithm for tethered satellites and the simulation of the control system with laboratory hardware. The control algorithm consists of a linear quadratic regulator feedback law and a Kalman filter. The control algorithm has been shown to regulate the vehicle orientation to within 0.60 arcsec rms. This level of precision was achieved only after including a mass center estimator and accurately modeling the effects of the nonlinear attach point motion actuator.

Introduction

THE advantages of and proposed uses for tethered configurations from both the Space Shuttle and space station have been well documented by Bekey.[1,2] A typical tethered satellite consists of two end masses connected with a long (1–100 km) flexible cable, which, for an orbiting system, is aligned with the local vertical. In this configuration, the constellation is dynamically stable due to gravity gradient restoring forces. Arnold[3] shows that the gravity (and centrifugal) gradient forces result in a relative acceleration away from the system mass center. This relative acceleration yields the microgravity environment typical of tethered satellites and the nominal tension force in the tether.

One use for which tethers are particularly well suited is to provide an isolation platform for space-borne observatories. The basic concept of tethering astrophysical pointing platforms is presented first by Lemke.[4] He qualitatively discusses the fact that tethered observatories will provide vibration and contamination isolation from the parent spacecraft and quantitatively designs a closed-loop attitude control system. The control algorithm he suggests makes use of a variable position tether attach point to generate control torques. He also discusses a proposed Space Shuttle flight test mission, called the Kinetic Isolation Tether Experiment (KITE), and presents a preliminary design and mission plan.

Lemke et al.[5] present an analysis of the attitude stability specifications for a typical astrophysical pointing platform. They determined that such a mission would require orientation control on the order of 1 arcsec. Furthermore, they analyze different methods to generate control torques and conclude that, to achieve orientation control to the required level, conventional means are inefficient and the control system must generate torques by varying the tether attach point on the tethered platform. This result arises because the force that the tether applies to the subsatellite is at least one order of magnitude greater than any other environmental disturbing force. If the tether is not attached exactly at the subsatellite mass center, a conventional control algorithm will expend too much energy fighting this (constant) disturbance torque. Further, the authors also discuss the KITE flight test configuration and hardware. They suggest that the mission include large-angle slew maneuvers on the order of 30 deg and inertially fixed pointing to exhibit long-term attitude regulation on the order of 1 arcsec.

Additional studies related directly to KITE appear in the open literature. Lemke[6] reviews the goals of the KITE project as they can be applied to the space station and adds a quantitative analysis of contamination isolation for a tethered observatory. Stephenson[7] performed a detailed computer simulation of the dynamics and control of a tethered observatory deployed from the Space Shuttle. He[8] presents results that provide a method to model the longitudinal and lateral dynamic behavior of long space-based tethers. In addition, He derives a three-dimensional, six-degree-of-freedom computer model and control algorithm based on generating control moments by varying the tether attach point. Both Stephenson and He concluded that the movable attach point control mechanism will, in fact, achieve orientation control on the order of 1 arcsec.

This paper extends the development of the aforementioned computer model control laws and presents results related to the ground-based verification of the KITE control concept. The key contribution of the analysis is to show that the largest sources of model uncertainty are imprecise knowledge of the mass center location and attach point motion modeling. A description of the experimental hardware that was constructed to serve as a test bed is provided. The test facility consists of an air-bearing supported vehicle suspended in a microgravity field and fitted with all of the necessary sensors, actuators, and electronics to implement a real-time controller. Finally, the results of a series of experimental tests are presented. The data show that the control concept based on a movable attach point can regulate tethered satellite orientation to within 1 arcsec.

Control Law Development

The attitude control system for a tethered astrophysical observatory must achieve long-term, high-accuracy (on the order of 1 arcsec) pointing to provide a stable platform for data collection. To achieve this, the control system must reject

Received July 29, 1991; revision received Feb. 12, 1992; accepted for publication March 1, 1992.

*Associate Research Scientist, O/92-30, B/250, 3251 Hanover St.
†Professor, Department of Aeronautics and Astronautics.

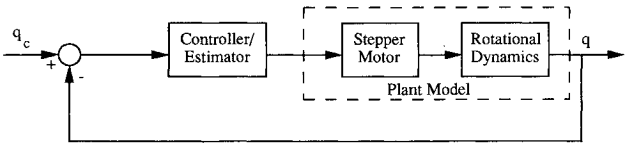

Fig. 1 Attitude control system block diagram.

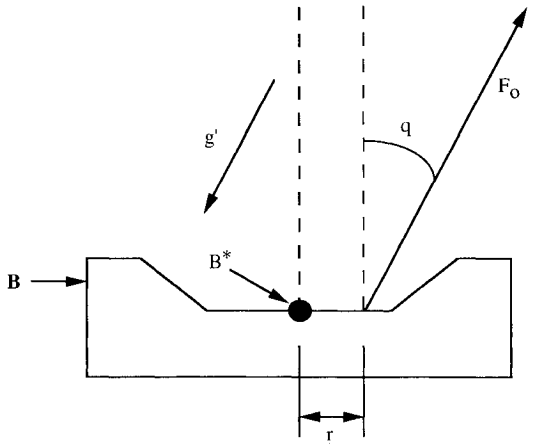

Fig. 2 Free body diagram of tethered subsatellite.

disturbances (both environmental and modeling errors) to the level that they will have a sufficiently small effect on the attitude of the satellite by increasing the dc gain of the control loop. A conceptual block diagram of the feedback control system is shown in Fig. 1. The figure shows that the system model (plant) consists of both the rotational dynamics of the subsatellite and the actuator dynamics (in this case, a stepper motor). The following sections present the equations of motion and control law development for the pitch dynamics of a tethered subsatellite.

Equations of Motion

The equation of motion that describes the rotational dynamics of a tethered subsatellite is quite simple (see Arnold[3]). A schematic free body diagram of a tethered subsatellite is shown in Fig. 2. The subsatellite B has a mass center B* located on the line of symmetry of the vehicle. The tether applies a force F_0 to the vehicle at the attach point, a distance r from B*. The angle q is the angular orientation of the vehicle with respect to the inertial reference frame defined by the nominal tether direction and is the angle that is to be controlled by the attitude control system. The magnitude of the microgravity field (which is a combination of two-thirds gravity gradient and one-third centrifugal acceleration) is given by g', and the direction is parallel to the nominal tether direction. The resultant gravity force acts at the mass center B*. The moment of inertia of the vehicle about an axis perpendicular to the plane of q and with respect to B* is given by I. Summing the torques applied to B yields the linearized rotational equation of motion for the air-bearing vehicle as:

$$I\ddot{q} = F_0 r \tag{1}$$

As shown in Fig. 1, the actuator for the closed-loop system is a stepper motor that drives a positioning table. The stepper motor is rigidly connected to the tether attachment, is a constant velocity device, and is nonlinear and difficult to model exactly. Figure 3 shows a typical closed-loop attach point position path. The position of the attach point may change during each sample period, but the magnitude of the attach point velocity is always the same. Because of the nature of the motion, a simple first-order lag has been used to describe the attach point motion. Therefore, the differential equation that describes the motion of the attach point can be written as follows:

$$\tau\dot{r} + r = r_d \tag{2}$$

where τ is the time constant of the lag model, r is the attach point position with respect to the assumed mass center, and r_d is the commanded attach point position as calculated by the control law.

Control Law

To achieve the high performance necessary in an attitude control system for an astrophysical pointing platform, a linear quadratic regulator (LQR) has been designed. In addition to the plant dynamics discussed earlier and to reject unmodeled disturbances, it is advantageous to include integral control in the control algorithm. A differential equation describing this integral state takes the following form:

$$\dot{e} = q \tag{3}$$

where e is the integral of the angular orientation of the subsatellite.

Equations (1-3) can be combined to form four first-order, linear, coupled differential equations of the form

$$\dot{x} = Fx + Gu$$

$$y = Hx \tag{4}$$

where $x = [q\ \dot{q}\ e\ r]^T$,

$$F = \begin{bmatrix} 0 & 1 & 0 & 0 \\ 0 & 0 & 0 & F_0/I \\ 1 & 0 & 0 & 0 \\ 0 & 0 & 0 & -1/\tau \end{bmatrix}$$

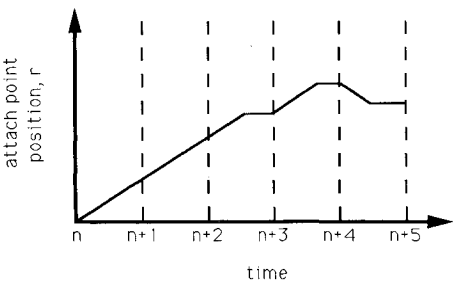

Fig. 3 Attach point time history.

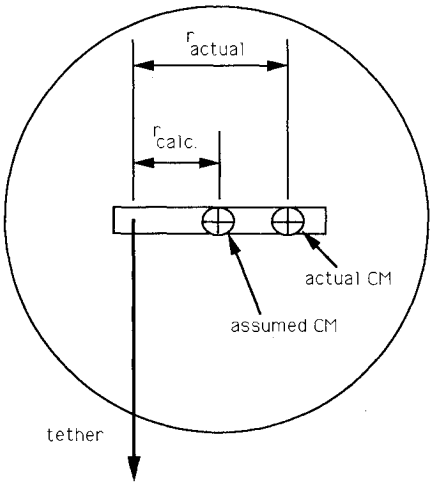

Fig. 4 Effect of mass center knowledge.

and where $G = [0\ 0\ 0\ (1/\tau)]^T$, $u = r_d$, and $H = [1\ 0\ 0\ 0]$. The value of F_0/I appropriate for the laboratory simulator can be shown to equal $(1/15)\text{m}^{-1}\text{s}^{-2}$ (Ref. 9). To perform the control law calculation, a standard quadratic performance index has been specified in the continuous domain using A and B as standard weighting matrices for the system state and control input, respectively. Feedback gains were calculated by converting the analog system model and performance index to an equivalent digital system. Then a standard routine for calculating digital feedback gains was invoked to perform the gain calculation with $\tau = 0.2$ s, $B = 1\ \text{m}^{-2}$, and $A = \text{diag}$ (100, 1, 5, 1), where the units of the elements in A are rad^{-2}, $(\text{rad/s})^{-2}$, $(\text{rad}\cdot\text{s})^{-2}$, and m^{-2}, respectively. The resulting calculation yields a feedback gain vector that corresponds to closed-loop root locations $z = 0.76 \pm 0.2j$, 0.89, -0.02.

State Estimator

To implement the digital control law, accurate knowledge of the values of all of the state variables must be available. Instead of separately measuring each of the states with a sensor, a single measurement, in addition to a state estimator, can yield the value of the state vector at each sample time. Three of the states can be determined without estimation. The error e is calculated using the simple digital equivalent of Eq. (3) and is given by

$$e_n = e_{n-1} + Ty_n \tag{5}$$

where e_n is the error and y_n is the angle measurement, respectively, at sample number n, and T is the sample period. The position and velocity of the attach point at each sample period are also available without estimation. The stepper motor is a digital device that receives shaft position commands limited to the maximum rotation it can achieve during a single time period. Therefore, at the beginning of the next sample period, the velocity is zero, and the position is equal to the commanded position at the previous sample time. The remaining states (q_n and $\dot{q}_n$) of the state vector are reconstructed with the measurement y_n of the angular orientation and the model of the system rotational dynamics.

To estimate the angular position and velocity of the vehicle accurately, it was necessary to estimate the vehicle center of mass as well. A priori knowledge of the location of the vehicle mass center is necessarily limited by our ability to measure this mass property accurately. Figure 4 shows the effect of imprecise knowledge of the location of the center of mass. If the control algorithm assumes the mass center to be located at a point that does not coincide with the actual mass center, the algorithm will calculate a desired position of the tether attach point (and will locate the attach point) with respect to the incorrect center of mass. After the tether is moved to that point, the actual torque applied to the vehicle will be different from the desired value. As a result, for the design of the state estimator, the equation describing the rotational dynamics of the vehicle should read

$$\ddot{q} = \frac{F_0}{I}(r + c) \tag{6}$$

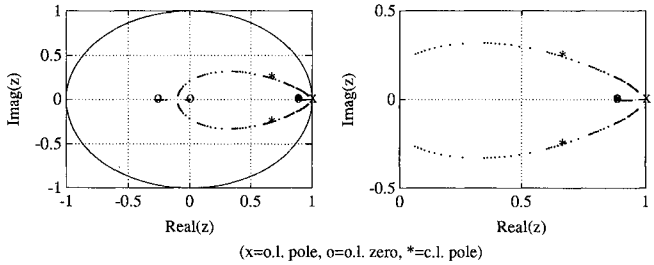

Fig. 5 Reciprocal root locus of state estimator.

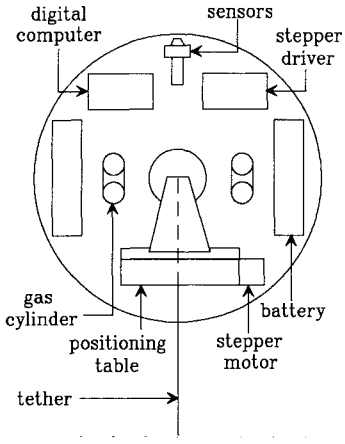

Fig. 6 Chassis component diagram.

where c is the difference between the actual center of mass and the assumed mass center. Therefore, three states (i.e., angular position, angular rate, and mass center location) must be estimated based on the single angular position measurement.

A convenient methodology to implement the state estimator is known as the Kalman filter (see Franklin and Powell,[10] Bryson and Ho,[11] and Powell[12]). The calculation of the filter gains for that portion of the state vector that needs to be estimated is based on the following set of differential equations:

$$\dot{x}_e = F_e x_e + G_d w$$

$$y_e = H_e x_e + v \tag{7}$$

where x_e is that part of the state vector to be estimated (i.e., $[q\ \dot{q}\ d]^T$),

$$F_e = \begin{bmatrix} 0 & 1 & 0 \\ 0 & 0 & -F_0/I \\ 0 & 0 & 0 \end{bmatrix}$$

and where G_d is the 3×1 disturbance input influence vector, y_e is the measurement, and $H_e = [1\ 0\ 0]$. The disturbance input w and the discrete equivalent of v are modeled as zero-mean white noise processes with spectral densities Q and R, respectively. The discrete Kalman filter gains can be calculated by first converting the system in Eqs. (7) into the equivalent discrete system and then invoking a standard estimator gain calculation package.

The result of the Kalman filter calculation is a 3×1 vector of gains L, which forms a software feedback system. To obtain some insight into the behavior of the estimator in the presence of varying process and measurement noise magnitudes, a reciprocal root locus was drawn numerically and is shown in Fig. 5. This was accomplished by varying the ratio of R and Q, performing the gain calculation, and determining the system pole locations for each value of the ratio. After a few iterations, it was found that the best estimator behavior could be realized by making the disturbance influence vector $G_d = [0\ 1\ 4]^T$. The pole locations that afforded the best combined controller-estimator performance correspond to a value of R/Q of 0.5 that yields estimator poles at $z = 0.88$, $0.66 \pm 0.25j$.

Experimental Equipment—Air-Bearing Vehicle

A detailed description of the air-bearing supported vehicle used to simulate a tethered pointing platform is presented by Kline-Schoder.[9] A brief review of the salient features of the air-bearing vehicle follows.

The pointing platform simulator consists of an air-bearing base plate that supports the necessary equipment to implement

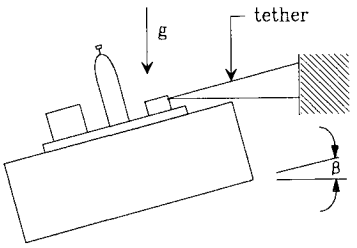

Fig. 7 Schematic side view of experimental setup.

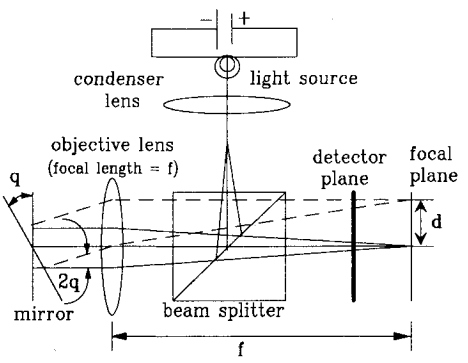

Fig. 8 Schematic of autocollimator optics.

an attitude control system that generates control torques by varying the tether attach point with respect to the vehicle mass center. The air-bearing support rides on a thin (approximately 75 μm) film of dry nitrogen gas on top of a very smooth granite table. A schematic diagram of the experimental hardware is shown in Fig. 6. The gas cylinders on board the vehicle are used to store the gas for flotation. The positioning table and stepper motor act as the mechanism that varies the tether attach point with respect to the vehicle mass center. The onboard electronics consist of a dc power supply, a digital computer, sensors, and the driver for the stepper motor. The individual components are arranged in a symmetric fashion about the center of the vehicle. This mounting style insures that the center of mass of the entire vehicle is very close to the center of the plate.

A schematic diagram of a side view of the experimental setup is shown in Fig. 7. This figure shows that the granite table is tilted at a small angle β with respect to the local horizontal. The table tilt results in a tether tension force that has the same characteristics as the microgravity field of the expected orbital case. The table tilt has been set such that $\beta \approx 2$ arcmin. This simulates the microgravity field experienced by a 2-km-long tethered satellite in a nominal 250-km altitude orbit. Because of obvious physical constraints in the laboratory, the use of a very long (2-km) tether is infeasible. Therefore, a 2-m-long piece of Spectra tether material is attached from the air-bearing vehicle to a nearby wall. Since a piece of long tether material is considerably more compliant than a short piece of material, a linear spring has been inserted between the tether and the wall attachment. This insures that unacceptably large tension variations are not generated by very small tether motions. The frequency of the mass-spring mode oscillation of the floating vehicle and tether/spring is approximately 0.30 Hz.

An autocollimator was used to measure the relative orientation of the air-bearing vehicle. A schematic diagram of the optical hardware for an autocollimator is shown in Fig. 8. The figure shows a condenser lens that serves to collect and focus the light from the integral light source. The beam of collected light then bounces off of the reflecting surface of a beam splitter and lands on the objective lens. The objective lens serves as a collimating lens for the light traveling away from the beam splitter. If q, the angle of the external mirror with respect to the collimated light, is zero, the collimated beam is reflected back on itself, passes through the objective lens heading back through the beam splitter (in the nonreflecting direction), and is focused as a point on the optical axis on the focal plane of the lens. If the mirror angle q is finite, the collimated beam is reflected from the mirror in an off-axis direction. The light then passes through the objective lens that focuses the beam on the focal plane at a distance d from the optical axis. The value of d can be shown to be:

$$d = (2q)f \tag{8}$$

where f is the focal length of the objective lens. By placing two photosensitive transistors along a plane parallel to the focal plane (with one just above the optical axis and one just below the optical axis), a linear measure of the relative angular position of the mirror and the autocollimator can be derived by comparing the relative amounts of light energy that fall on each detector. The autocollimator used in this study was developed by Lorell[13] for the work he did in the precision attitude control of spinning bodies. The static output of the autocollimator possesses an rms noise level of 0.75 arcsec and a dynamic range of ± 0.5 deg.

Experimental Results

The tethered satellite laboratory simulator has been used to perform an extensive study of the attitude control system just discussed. The purposes of the study were to test the theoretical results presented earlier and to determine the effect that hardware characteristics will have on the performance of the system. This includes determining the effects of estimation, stepper motor modeling, and linearity assumptions (which are related to longitudinal and lateral tether dynamics). All of the experiments have been performed such that finite initial conditions were reduced to zero.

Fine Pointing Control

The requirements for a modern space-based telescope are such that attitude stability on the order of 1 arcsec is necessary

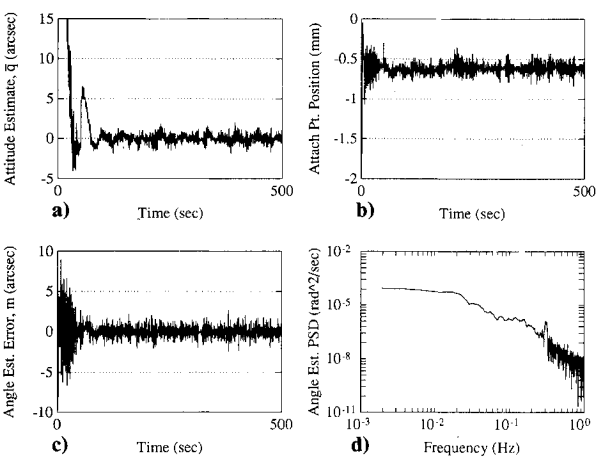

Fig. 9 Typical fine pointing results.

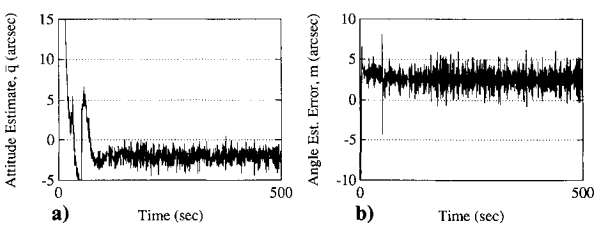

Fig. 10 Results without mass center estimation [with center of mass (CM) error of 0.4 mm].

to fulfill typical mission requirements. A series of experiments were performed to test the ability of the control algorithm to provide a long-term high-accuracy pointing platform as a base for astrophysical observations. The goal of these tests was to determine the best possible behavior in a configuration free of environmental disturbances. These results serve as the basis from which observed behavior in the presence of realistic disturbance forces can be judged (see Ref. 9).

Results of a typical fine pointing attitude control experiment are shown in Fig. 9. This figure shows the time histories of the estimate of the vehicle orientation $\bar{q}(n)$, the attach point position (with respect to the assumed mass center), the error in the time update estimate of the angle $m(n) = q(n) - \bar{q}(n)$, and the power spectral density of the estimated attitude. The time history of the estimated vehicle orientation (Fig. 9a) shows that the initial orientation (approximately 80 arcsec) is reduced to a narrow band of values about the 0 arcsec measure in 100 s. The peak time is 25 s, and the overshoot is approximately 5%. This corresponds to a closed-loop bandwidth of approximately 0.03 Hz. The rms value of the measured attitude from 20–500 s is 0.60 arcsec, and the average value over that time period is 6.6×10^{-3} arcsec. The attach point time history (Fig. 9b) shows that, after an initial large step to start the angular motion, the position returns to a narrow band of values about the -0.6-mm measure. The random motion of the position is a result of the control algorithm reacting to sensor noise, and the nonzero steady-state average value is the result of a difference between the assumed and actual mass center locations (as is calculated by the mass center estimator). The error in the time update estimate of the angle (Fig. 9c) shows that, after the first 100 s, the estimate converged to the measured value (within sensor limitations). The rms value of the error for the time between 200–500 s can be calculated to be 0.75 arcsec, and the average value during that time period is 7.5×10^{-4} arcsec. The power spectral density of the angle estimate (Fig. 9d) shows a flat function for frequencies below the bandwidth and attenuation for frequencies above the bandwidth. Also, the mass-spring mode of the air-bearing vehicle and tether/spring system is clearly evident through the relatively large spike at 0.3 Hz. These observed results compare quite well with the theoretical results obtained previously. The bandwidth and damping correlate to within 10% of the previously predicted values.

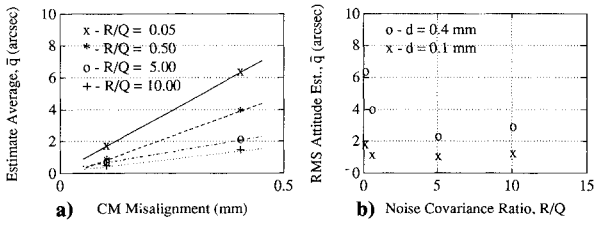

Fig. 11 Summary of results without CM estimation.

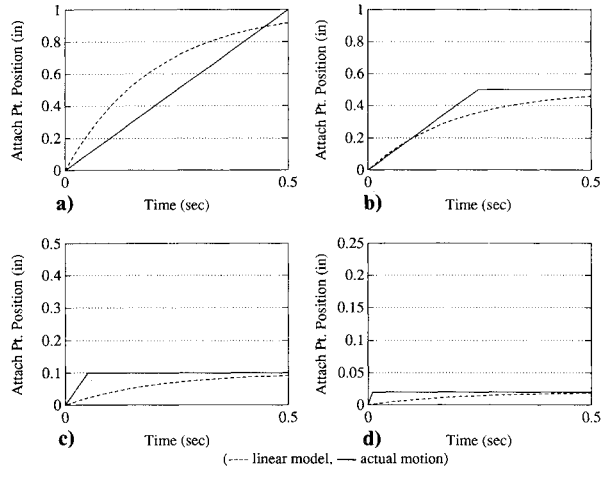

Fig. 12 Comparison of stepper motion to linear model.

Table 1 Effect of estimator gains on rms performance (nominal $R/Q = 0.5$)

R/Q	$\bar{q}(n)$, arcsec	$m(n)$, arcsec
0.01	1.11	1.07
0.05	0.86	0.75
0.10	0.71	0.74
0.50	0.60	0.75
1.00	0.70	0.94
5.00	0.78	1.58
10.0	0.84	1.98

Effect of Estimator Gains

The previous discussion of the derivation of the state estimator showed how the process and sensor noise models played a key role in determining the numerical values of the estimator feedback gains. To determine the effect that different assumed values for the ratios of the sensor to process noise covariances would have on the closed-loop system performance, a series of tests were performed where the noise covariance ratio (i.e., R/Q) was varied for purposes of computing the estimator gains. Increasing the covariance ratio causes the estimator to converge to the actual state value more rapidly, but the faster convergence can amplify the sensor noise unnecessarily. The goal, then, is to choose estimator root locations that allow timely state convergence yet maintain reasonable sensor noise filtering. This balancing is most easily performed with an extremely accurate system model and was the motivation behind the mass center estimator discussed earlier.

Results of the different tests performed with the experimental system and varying values of estimator gains are summarized in Table 1. This table shows the ratio of sensor noise covariance to process noise covariance R/Q used in the estimator gain calculation, the rms value of the steady-state estimate of angular orientation $\bar{q}(n)$, and the rms value of the error in the estimate of angular orientation before the measurement, $m(n) = q(n) - \bar{q}(n)$. The estimate of the angular orientation gives a quantitative measure of the performance of the closed-loop system (i.e., control law and estimator), and the error in the estimate of the angular orientation before the measurement provides a quantitative measure of the performance of the estimator implementation. The results shown in the table support the thesis that varying sensor and process noise models will affect the behavior of the estimator and closed-loop system. Small values of the covariance ratio result in relatively poor estimator and closed-loop system performance. This results from the slow (sluggish) response time of the estimator and too great a reliance on a model that is not 100% accurate. Large values of the covariance ratio also result in relatively degraded performance. This results because of the small amount of sensor noise filtering provided by an estimator with a relatively fast (quick) response time. The midrange values of those shown result in fairly equal estimator performance but slightly different closed-loop system behavior. The performance of the estimators are all basically equivalent because they filter sensor noise roughly equally. The closed-loop system behavior is different because of the location of the estimator roots with respect to the controller root locations. For the 0.01, 0.05, and 0.10 values of R/Q, the estimator root locations correspond to an estimator that is slower than the controller roots, whereas when $R/Q \geq 0.50$, the estimator roots correspond to an estimator that is faster than the controller. An estimator that is slower than the controller can cause slightly degraded closed-loop performance in the response to step commands and unmodeled disturbances be-

Table 2 Summary of tests varying motor time constant

τ, s	$\bar{q}(n)_{rms}$, arcsec	$m(n)_{rms}$, arcsec
0	1.59	1.26
0.01	0.75	1.06
0.02	0.73	0.98
0.20	0.60	0.75
2.00	0.66	1.24
4.00	0.70	1.32

cause the control calculation will be based on a state estimate that does not respond as quickly as the controller responds.

Effect of Mass Center Estimation

The preceding derivation of the state estimator includes a qualitative argument justifying the need for estimation of the center of mass of the subsatellite. To quantitatively determine the effect of the mass center estimator, a series of tests were performed without the implementation of the mass center estimator. The center of mass of the vehicle was accurately located (to within 0.05 mm) with respect to the center of the vehicle base plate. Then, for purposes of this study, the mass center location was assumed to be different from the known location. Two tests were performed, one with an intentional mass center misalignment of approximately 0.10 mm and the other with the misalignment intentionally set to 0.40 mm. The control gains were made the same as those discussed earlier. The estimator, without mass center estimation, can be derived by changing the value of the disturbance influence vector given in Eqs. (7) to $\boldsymbol{G}_d = [0\ 1\ 0]^T$. The effect of this change on the estimator is that, since there is no model of process noise disturbing the location of the mass center, the Kalman filter will assume that the initial location is, in fact, the actual mass center location (effectively an oblivious filter) and the estimator gain associated with this state will be zero. Experiments were performed with estimator gains calculated from various covariance ratios in an effort to judge the effect of estimator speed of response in addition to the mass center estimation.

Results of these tests are summarized in Figs. 10 and 11. Figure 10a shows the closed-loop attitude angle estimate before the measurement $\bar{q}(n)$, and Fig. 10b shows the error in the estimate before the measurement $m(n) = [q(n) - \bar{q}(n)]$ as a function of time for the experiment with an intentional mass center misalignment c equal to 0.40 mm and a value of R/Q equal to 5.0. As expected, the mass center misalignment caused the control algorithm to calculate attach point locations that did not provide the necessary control torques to zero the attitude of the vehicle. For the time between 200 and 500s, the average value of the attitude estimate is -2.05 arcsec, the rms value of the attitude estimate is 2.21 arcsec, and the rms value of the error in the angle estimate is 2.86 arcsec. This is in sharp contrast to the comparable values obtained for the case with the mass center estimator. The degradation in performance results from the fact that the actual control torque applied to the vehicle differs from the desired value because of the mass center misalignment.

Figures 11a and 11b show the absolute value of the angle estimate before the measurement $\bar{q}(n)$ as a function of mass center misalignment for various values of the noise covariance ratio R/Q and the rms value of the attitude estimate before the measurement $\bar{q}(n)$ as a function of noise covariance ratio for two values of mass center error c. The values shown in the figures make physical sense. The tests performed with a smaller mass center misalignment would be expected to show better behavior than the case where the center of mass misalignment was larger. The smaller the misalignment, the smaller the difference between the actual and desired control torques, the smaller the error in estimating the state. This should yield smaller mean square and average values of the attitude error. In addition, higher estimator gains (which correspond to a higher noise covariance ratio) force the Kalman filter to rely less on the system model and more on the given measurement. A de-emphasis of the model will produce smaller estimator errors, translating into better performance. It should be noted, however, that blindly increasing the gains of the estimator can have detrimental effects, as can be seen in Fig. 11b. Increasing the covariance ratio benefits the operation of the control system until the ratio approaches a value of approximately 5. At this point, the estimator is amplifying the noise in the measurement unnecessarily. The purpose of low estimator gains is to filter the noise of the measurement by balancing the knowledge gained from each measurement with the system model. A very accurate system model allows lower gains and, therefore, more filtering of the measurement. A good estimator will possess the lowest possible gains (the highest possible filtering) and the most accurate model available.

It should be noted that the mass center misalignments measured in the laboratory are quite small with respect to a characteristic dimension of the vehicle (on the order of 0.01 and 0.04%, respectively). For a realistic satellite implementation, a 1% characteristic dimension misalignment would not be unexpected. As a result, the effect of mass center misalignment in a practical application can be on the order of 100 times greater than the effect measured in the laboratory (i.e., on the order of 100 arcsec). Clearly, mass center estimation should be an integral part of a high-accuracy tethered satellite attitude control system that generates control torques by varying the attachment of the tether with respect to the mass center of the vehicle.

Effect of Stepper Motor Model

The linear model of the stepper motor discussed in Fig. 3 qualitatively summarizes the need for attach point motion modeling. The linear model chosen to represent the dynamics of stepper motor motion is shown in Eq. (2) to be a simple first-order lag that is characterized by the time constant τ. In an effort to determine the quantitative effects of varying the model of the stepper motor dynamics, a series of tests were performed with compensators designed by assuming various values of the time constant. When designing a compensator, the value of τ affects both the feedback control gains K and the control influence vector $\boldsymbol{\Gamma}$. The feedback gains were calculated with the same state and control weighting matrices (A and B, respectively) as the nominal case discussed earlier.

The results of these tests are shown in Table 2. The table shows that varying the time constant of the stepper motor does indeed affect the behavior of the closed-loop system and the performance of the state estimator. The best response is obtained when $\tau = 0.2$ s. The worst response, as can be expected, corresponds to the case where the dynamics of the stepper motor are ignored (i.e., $\tau = 0$ s). All other values of τ that were tested resulted in closed-loop systems with measured angle rms values that are less than 1 arcsec. However, the estimator performance, as judged by the rms value of the error in the angle estimate before the measurement, was affected to a greater extent. The increase in sensitivity of the estimator is because varying the model varies how well the model represents the physical mechanism, and since the angle estimate before the measurement was used to compare the model performance, the sensitivity is heightened. The control input, on the other hand, is calculated based on the state estimate after the measurement, which is the less model sensitive (because of the information contained in the measurement) of the time and measurement update state vectors.

Figures 12a–12d provide a visual representation of the physical significance of modeling the nonlinear stepper motor with a linear differential equation. The figures show the actual motion of the attach point and the attach point motion modeled as a low pass filter (with $\tau = 0.2$ s) for cases when the desired motion during one sample period takes on the values of 1.0 in. (Fig. 12a), 0.5 in (Fig. 12b), 0.1 in (Fig. 12c), and 0.02 in (Fig. 12d). The figures show that the model is not an

exact representation of the attach point motion and that the differences between the actual and modeled motion depend on the size of the desired motion. This tendency arises due to the strong dependency of the actual motion on the size of the input. The results and discussion emphasize the fact that care must be taken when modeling nonlinear devices with linear differential equations.

Discussion

The unique dynamic characteristics of tethered spacecraft make them well suited to serve as isolation platforms for space-based observatories. For missions requiring better than 1 deg long-term stability, conventional means of performing the orientation control of a tethered subsatellite are ineffective because of the relatively large tension force applied to the satellite by the tether. It has previously been shown that generating control torques by varying the tether attach point with respect to the subsatellite mass center is not only effective but also necessary for missions with attitude stability requirements on the order of 1 arcsec. The implemented pointing control algorithm was based on a linear quadratic regulator feedback law and a Kalman filter. The control law includes the integral of the vehicle orientation angle as an augmented state and an approximation of the dynamics of the nonlinear actuator (used to position the tether attach point). The Kalman filter includes the rotational dynamics of the satellite, plus a mass center estimator that is used to calculate, in real time, the actual position of the subsatellite center of mass.

A laboratory simulator of a tethered satellite has been designed and constructed. The simulator consists of an air-bearing vehicle on which all of the necessary hardware to implement the attitude control algorithm has been mounted. The air-bearing vehicle is suspended in a microgravity field (by tilting the table on which it floats with respect to local gravity) and connected with a tether to a nearby wall. Pointing control experimental results showed that an initial angular displacement was reduced to 0.60 arcsec rms in less than 100 s. The closed-loop bandwidth is approximately 0.03 Hz with overshoot on the order of 5%. The state estimator functioned in such a way that the estimate of the angular orientation had an rms value of 0.75 arcsec, which is sensor limited. These results agree to within 10% of the theoretical analysis and computer simulation of the closed-loop system.

Further tests were performed to judge the effect of the magnitude of the estimator gains, the need for the mass center estimator, and the effect that various actuator models had on the steady-state control algorithm behavior. The results show that the magnitude of the estimator gains (i.e., the ratio of sensor and process noise models) do have an effect on the system performance. Relatively poor estimator and system performance were observed for estimator gains that corresponded to too great a reliance on the measurement or too great a reliance on the model. Estimator gains based on a proper balance between sensor and process noise exhibited acceptable estimator performance. In addition, if the estimator root locations corresponded to faster response times than the control root locations, the closed-loop system behaved quite well. The results of the tests of the mass center estimator showed that mass center estimation is necessary for a precision tethered satellite attitude control system based on a movable tether attach point. The magnitude of the effect of not estimating the mass center location was found to depend on the magnitude of the estimator gains and the misalignment between the assumed and the actual mass center locations. The results related to the model of the nonlinear actuator emphasized the fact that care must be taken when modeling nonlinear devices with linear equations.

Conclusions

A laboratory simulator of a tethered pointing platform has been built and was used to evaluate the performance of an attitude control system based on a movable tether attachment. It was found that the two main effects that limit controller performance are modeling of the tether attachment point dynamics and accurate knowledge of the subsatellite mass center location. Including an accurate model of the attachment point dynamics reduces the estimate errors by approximately a factor of two and developing a center of mass estimator reduces the estimator errors to a sensor noise limited value. For the angle sensor used in these studies, a pointing accuracy of 0.60 arcsec rms was achieved with the experimental hardware.

Acknowledgments

The research for this paper was supported by the NASA Ames Research Center under Grant NCC 2-389. The authors would like to acknowledge the contributions of Lawrence Lemke of NASA Ames Research Center. He was principally responsible for securing funding for the research presented in this paper and provided the original control concept studied herein. Additionally, Harold Alexander and Russ Hacker played key roles in the development of the experimental hardware.

References

[1]Bekey, I., "Tethers Open New Space Options," *Astronautics and Aeronautics,* Vol. 21, No. 4, 1983, pp. 33-40.

[2]Bekey, I., "Space Station Operations Enhancement Using Tethers," 35th Congress of the International Astronautical Federation, IAF-84-43, Lausanne, Switzerland, Oct. 1984.

[3]Arnold, D. A., "The Behavior of Long Tethers in Space," *The Journal of the Astronautical Sciences,* Vol. 35, No. 1, 1987, pp. 3-18.

[4]Lemke, L. G., "A Concept for Attitude Control of a Tethered Astrophysical Observatory Platform," *Proceedings of the AIAA Guidance, Navigation, and Control Conference* (Snowmass, CO), AIAA, New York, 1985.

[5]Lemke, L. G., Powell, J. D., and He, X., "Attitude Control of Tethered Spacecraft," *The Journal of the Astronautical Sciences,* Vol. 35, No. 1, 1987, pp. 41-56.

[6]Lemke, L. G., "Preliminary Feasibility Study of Observatory Platforms Tethered to Space Stations," Engineers Thesis, Dept. of Aeronautics and Astronautics, Stanford Univ., Stanford, CA, 1990.

[7]Stephenson, M. W., "Dynamics and Control of the Space Shuttle-Based Kinetic Isolation Tether Experiment," Master of Science and Engineers Thesis, MIT, Cambridge, MA, 1988.

[8]He, X., "Attitude Control of Tethered Satellites," Ph.D. Thesis, Dept. of Aeronautics and Astronautics, Stanford Univ., Stanford, CA, 1990.

[9]Kline-Schoder, R. J., "Precision Tethered Satellite Attitude Control," Ph.D. Thesis, Dept. of Mechanical Engineering, Stanford Univ., Stanford, CA, 1990.

[10]Franklin, G. F., and Powell, J. D., *Digital Control of Dynamic Systems,* Addison-Wesley, Reading, MA, 1981.

[11]Bryson, A. E., and Ho, Y. C., *Applied Optimal Control,* Hemisphere, Washington, DC, 1975.

[12]Powell, J. D., "Mass Center Estimation in Spinning Drag-Free Satellites," *Journal of Spacecraft and Rockets,* Vol. 9, No. 6, 1972, pp. 399-405.

[13]Lorell, K., "Precision Attitude Control of Symmetric Spinning Bodies," Ph.D. Thesis, Dept. of Aeronautics and Astronautics, Stanford Univ., Stanford, CA, 1971.